Magnetoelectric coupling and phase transition in BiFeO3 and (BiFeO3)0.95(BaTiO3)0.05 ceramics

T.-H. Wang, C.-S. Tu, H.-Y. Chen, Y. Ding, T. C. Lin, Y.-D. Yao, V. H. Schmidt, and K.-T. Wu

Citation: Journal of Applied Physics **109**, 044101 (2011); doi: 10.1063/1.3551578
View online: http://dx.doi.org/10.1063/1.3551578
View Table of Contents: http://scitation.aip.org/content/aip/journal/jap/109/4?ver=pdfcov
Published by the AIP Publishing

Magnetoelectric coupling and phase transition in $BiFeO_3$ and $(BiFeO_3)_{0.95}(BaTiO_3)_{0.05}$ ceramics

T.-H. Wang,[1] C.-S. Tu,[1,2,a)] H.-Y. Chen,[2] Y. Ding,[1,3] T. C. Lin,[2] Y.-D. Yao,[1] V. H. Schmidt,[4] and K.-T. Wu[1,2]
[1]*Graduate Institute of Applied Science and Engineering, Fu Jen Catholic University, Taipei 242, Taiwan*
[2]*Department of Physics, Fu Jen Catholic University, Taipei 242, Taiwan*
[3]*Teaching Center of Natural Sciences, Minghsin University of Science and Technology, Hsinchu 304, Taiwan*
[4]*Department of Physics, Montana State University, Bozeman, Montana 59717, USA*

(Received 17 June 2010; accepted 23 December 2010; published online 23 February 2011)

In situ high-resolution synchrotron x-ray diffraction reveals a local minimum in rhombohedral distortion angle α_R (associated with an inflection in the lattice constant a_R) near 400 and 350 °C in $BiFeO_3$ (BFO) and $(BiFeO_3)_{0.95}(BaTiO_3)_{0.05}$ (BFO–5%BT), respectively. It suggests a coupling between ferroelectric and magnetic parameters near the antiferromagnetic–paramagnetic transition, which is responsible for the broad frequency-dependent dielectric maxima. A rhombohedral (R)–orthorhombic (O)–cubic (C) transition sequence takes place near 820 and 850 °C in BFO upon heating. BFO–5%BT exhibits a R–C transition near 830 °C. The $BaTiO_3$ substitution can enhance dielectric and ferromagnetic responses and reduce electric leakage. The dielectric loss of BFO–5%BT remains less than 0.04 below 150 °C. © *2011 American Institute of Physics*. [doi:10.1063/1.3551578]

I. INTRODUCTION

The multiferroic bismuth ferrite $BiFeO_3$ (BFO) materials have attracted much attention not only because they possess ferroelectric (FE) and ferromagnetic (FM) properties, but also because the coupling between the electric and magnetic ordering leads to additional functionalities.[1–3] BFO can provide an alternate choice as a "green" FE/FM material as compared with lead-containing compounds, such as $Pb(Zr_xTi_{1-x})O_3$ (PZT), $Pb(Mg_{1/3}Nb_{2/3})O_3$–$PbTiO_3$, and $Pb(Zn_{1/3}Nb_{2/3})O_3$–$PbTiO_3$.[4] BFO has a high FE Curie temperature ($T_C = 810$–870 °C) and antiferromagnetic Néel temperature ($T_N = 352$–397 °C),[5–13] which enable it to be used reliably above room temperature.

A rhombohedral structure of *R3c* space group ($a_R = 5.616$ Å and $\alpha_R = 59.35°$) was reported for bulk BFO at room temperature,[14] but can also be indexed based on the pseudocubic lattice ($a_{pc} = 3.96$ Å).[15] The dielectric results of BFO–PZT solid solutions predicted a FE Curie temperature near 850 °C for the pure BFO.[13] From Raman scattering and differential thermal analysis, a rhombohedral–orthorhombic–cubic phase sequence was observed near 820 and 925 °C upon heating in bulk BFO.[16,17] However, a monoclinic–orthorhombic–cubic was proposed in (001) BFO thin film.[16] The recent powder neutron diffraction result of BFO revealed a phase sequence of rhombohedral-β orthorhombic-γ orthorhombic.[18]

The spontaneous polarization of bulk BFO was expected to be 90–110 $\mu C/cm^2$, predicted by *ab initio* calculations[19,20] because of large atomic displacement. Spontaneous polarizations of 60 and 40 $\mu C/cm^2$ were reported in BFO crystal and ceramic, respectively.[21,22] However, most reported BFO ceramics exhibit small electric polarization and nonsaturated hysteresis loops,[9,23,24] which were attributed to electric leakage. It has been a challenge to synthesize high-density BFO ceramics, because a second phase or impurity can easily result. To reduce electric leakage, many studies have focused on doped BFO ceramics with ion substitutions to enhance magnetic and electric properties.[25–29] The structures of $(1-x)BiFeO_3$–$xBaTiO_3$ solid solutions are rhombohedral, cubic, and tetragonal for, respectively, $0 \le x \le 0.33$, $0.33 \le x \le 0.925$, and $x > 0.925$ in the low temperatures.[30,31]

Although BFO has been studied extensively in recent years, its phase transition, dielectric properties, and magnetoelectric coupling still lack consistency and are not fully understood. The main focus of this work is to study phase transitions and magnetoelectric coupling of BFO and $(BiFeO_3)_{0.95}(BaTiO_3)_{0.05}$ (BFO–5%BT) ceramics by *in situ* high-resolution synchrotron x-ray diffraction (XRD). Another task is to examine the $BaTiO_3$-substitution effect on dielectric and magnetic properties.

II. EXPERIMENTAL PROCEDURES

The BFO ceramic was prepared by the solid state reaction method. The dried starting powders of Bi_2O_3 and Fe_2O_3 (purity $\ge 99.0\%$) were weighed in a 1.1:1 ratio to compensate the low melting point of Bi, and then mixed in an agate mortar for more than 24 h using alcohol as a medium. The mixture was dried and mixed with polyvinyl acetate as a binder for granulation. The ground mixture was pressed into a 1.0-cm-diameter disk. The pressed BFO disk was sintered in the region of 850–870 °C for 1–3 h. The optimal sintering condition for BFO ceramic is 860 °C for 2 h and the density is ~90% of the theoretical density. For synthesis of BFO–5%BT ceramic, the dried starting powders of BFO and BT (purity $\ge 99.0\%$) were weighed in a 0.95:0.05 molar ratio

a)Author to whom correspondence should be addressed. Electronic mail: 039611@mail.fju.edu.tw.

and then a similar process was followed as for the BFO ceramic. The optimal sintering condition for BFO–5%BT ceramic is 960 °C for 3 h and the density is ~93% of the theoretical density.

In situ high-resolution synchrotron XRD was performed at the National Synchrotron Radiation Research Center (in Taiwan) with a photon energy of 8.0 keV ($\lambda = 1.550$ Å). A Wayne–Kerr Analyzer PMA3260A was used to obtain the real (ε') and imaginary (ε'') parts of dielectric permittivity. Hysteresis loops of polarization versus E field were taken by using a Sawyer-Tower circuit at $f = 46$ Hz.

III. RESULTS AND DISCUSSION

Figure 1 shows XRD spectra of BFO and BFO–5%BT ceramics at room temperature. A two-peak splitting occurs in the (110), (111), (210), and (220) reflections, suggesting a rhombohedral structure.[32] Some minor second phases (impurity) of possible $Bi_{25}FeO_{39}$ (Ref. 21) and $Bi_2Fe_4O_9$ (Ref. 33) were observed as indicated by the symbols "*" and "#," respectively. BFO–5%BT has less impurity phases. The XRD peaks of BFO–5%BT occur at lower 2θ than those in BFO, mainly due to the larger atomic radius of the Ba^{2+} ion (1.35 Å) compared with the Bi^{3+} ion (1.03 Å) on the perovskite A site. The Fe^{3+} ion (0.64 Å) and Ti^{4+} ion (0.605 Å) have similar atomic radii on the perovskite B site.

Figure 2 shows frequency-dependent dielectric permittivity (ε') and dielectric loss ($\tan\delta = \varepsilon''/\varepsilon'$) upon heating. The temperature (T_m) corresponding to the maximum in ε' exhibits a broad frequency dispersion. For BFO, T_m shifts from ~420 °C at 50 kHz to ~490 °C at 1 MHz. BFO–5%BT does not exhibit obvious frequency dispersion in ε' below 200 °C and its T_m shifts to lower temperatures. This dielectric response is likely activated by the antiferromagnetic–paramagnetic transition, which takes place at the Néel temperature (T_N).[5–13] A similar but rather pronounced frequency dispersion in dielectric maxima was observed in BFO–10%BT ceramic, associated with a local minimum in rhombohedral distortion angle α_R near T_N.[29] It was attributed to the changes in relative positions of Bi^{3+} and Fe^{3+} ions in the perovskite structure as temperature approaches T_N. In addition, the neutron scattering result of BFO also revealed changes of distortion and strain in oxygen octahedra (FeO_6) at T_N caused by the magnetoelectric and/or magnetoelastic couplings,[8] which can change electric polarization.

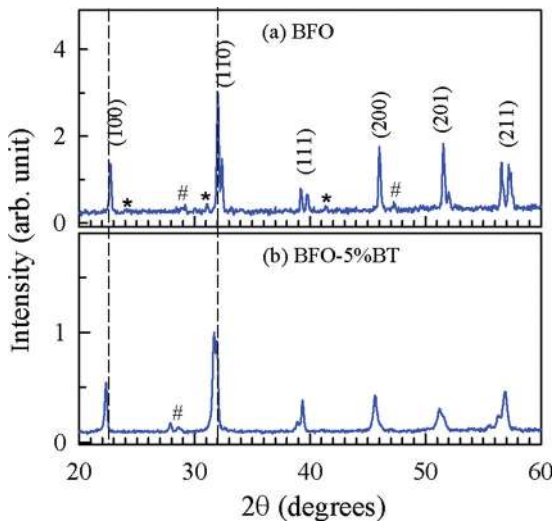

FIG. 1. (Color online) XRD spectra of (a) BFO and (b) BFO–5%BT at room temperature. "*" and "#" correspond to second phases of possible $Bi_{25}FeO_{39}$ and $Bi_2Fe_4O_9$. The dashed lines indicate 2θ shifts between BFO and BFO–5%BT.

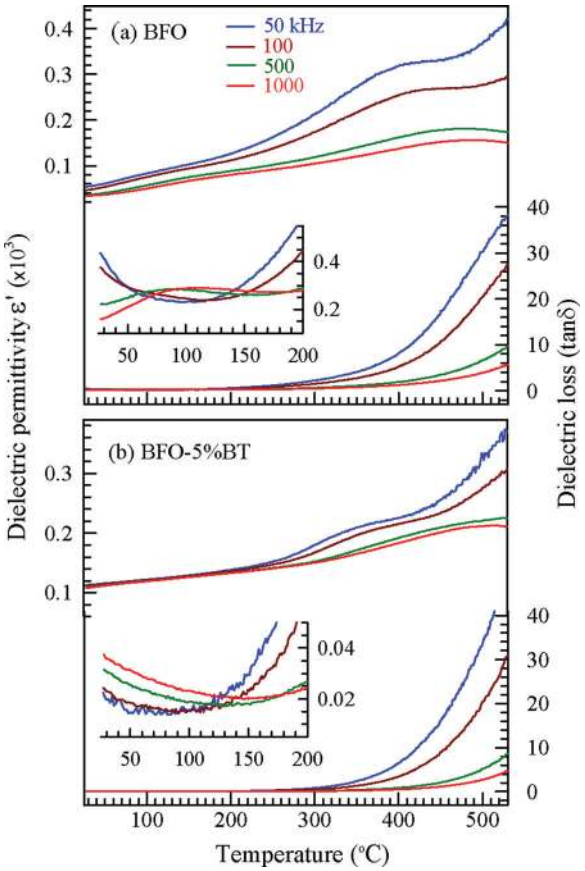

FIG. 2. (Color online) Dielectric permittivity ε' and loss ($\tan\delta$) of (a) BFO and (b) BFO–5%BT upon heating. (Insets) Enlargements of loss below 200 °C.

The dielectric loss ($\tan\delta$) of BFO and BFO–5%BT are respectively about 0.2–0.4 and 0.02–0.04 at room temperature, indicating that 5 mol % $BaTiO_3$ substitution can efficiently reduce electric conductivity. The tan δ of BFO–5%BT remains less than 0.04 below 150 °C, which is close to the $\tan\delta \cong 0.02$ of the soft PZT-5 ceramic.[34] The dielectric losses of BFO and BFO–5%BT exhibit an exponential upturn above ~300 °C with magnitude proportional to $1/f$, indicating conductivity activated by thermal energy.

Figure 3 shows temperature-dependent (110) synchrotron XRD spectra of BFO and BFO–5%BT upon heating. The insets are the XRD spectra near structural transitions. The (110) XRD spectrum of BFO–5%BT is much broader than in BFO, likely caused by random distributions of Bi and Ba ions on the A site, and Fe and Ti ions on the B site. The random displacements can cause different 2θ reflections and result in a broadening effect in XRD. Upon heating, two (110) R-phase reflections of BFO exhibit a triple splitting near 820 °C and then merge into a single peak near 850 °C, indicating a transition sequence of rhombohedral (R)–

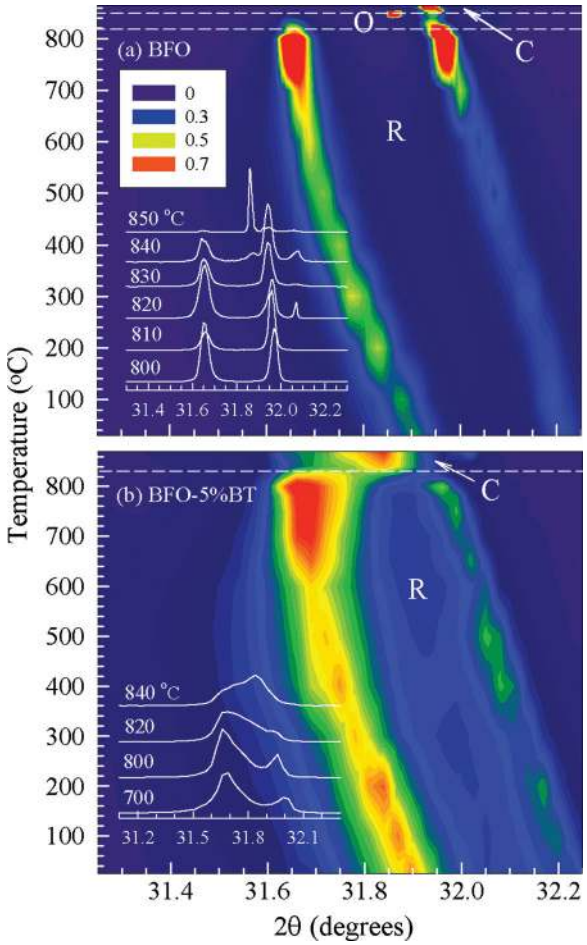

FIG. 3. (Color online) The (110) synchrotron XRD spectra of (a) BFO and (b) BFO–5%BT upon heating. (Insets) XRD spectra near structural transitions. The dashed lines indicate the transition temperatures.

orthorhombic (O)–cubic (C) upon heating. A R–O–C phase sequence was also revealed in bulk BFO near 820 and 925 °C from Raman and thermal studies.[16] Our result is consistent with the dielectric result of BFO–PZT solid solutions, which predicted a ferroelectric Curie temperature near 850 °C for BFO.[13] Additional XRD peaks appear above 860 °C in BFO, implying possible decompositions of Fe_2O_3 and $Bi_2Fe_4O_9$ (Ref. 33) due to the loss of Bi in high-temperature region.

For BFO–5%BT, two (110) R-phase reflections merge into a broad single peak near 830 °C, indicating a rhombohedral (R)–cubic (C) transition upon heating. This result may imply that the orthorhombic phase is not favored by replacing $BaTiO_3$ in the perovskite structure. Decomposition does not occur in BFO–5%BT below 900 °C, implying that 5%BT substitution can stabilize the perovskite structure.

Figure 4 shows temperature-dependent lattice parameters calculated from the (110) XRD peaks. A local minimum in rhombohedral distortion angle α_R (associated with a slight inflection in lattice constant a_R) occurs near 400 and 350 °C in BFO and BFO–5%BT, respectively. A similar minimum of α_R was reported near T_N in BFO and BFO–10%BT.[29,35] This local minimum in α_R suggests that the position shift (or distortion) of Bi^{3+} cation gradually reaches a maximum as temperature approaches T_N. This confirms a coupling

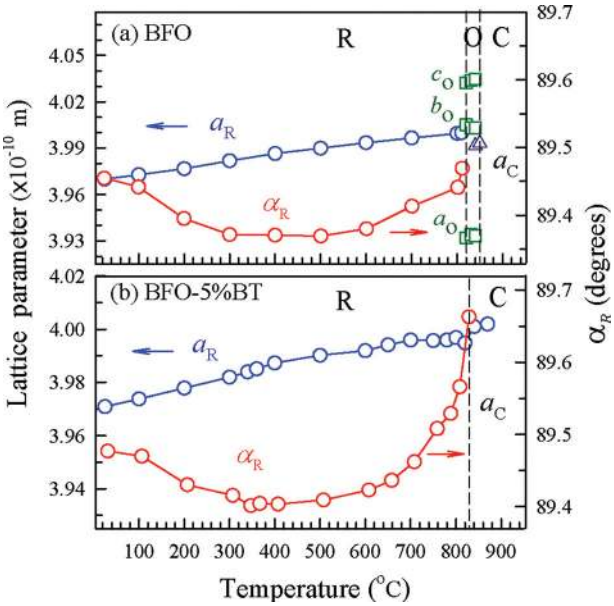

FIG. 4. (Color online) Temperature-dependent lattice parameters of (a) BFO and (b) BFO–5%BT. a_R, α_R, and a_C are lattice parameters of rhombohedral (R) and cubic (C) structures and a_O, b_O, and c_O are lattice constants of orthorhombic (O) structure. The lattice parameters were calculated based on the pseudocubic lattice.

between ferroelectric and magnetic order parameters near T_N, which causes the broad frequency-dependent dielectric maxima as shown in Fig. 2.

Electric hysteresis loops at room temperature are given in Fig. 5 and show attainable remanent polarizations of ~0.01 and ~0.1 $\mu C/cm^2$ in BFO and BFO–5%BT, respectively. However, the saturated polarization cannot be achieved in either case. A similar hysteresis loop with an unsaturated remanent polarization of ~0.01–0.015 $\mu C/cm^2$ was observed from the BFO ceramic.[9] As evidenced in Fig. 5, BFO–5%BT can sustain a higher measuring field than BFO, confirming that 5%BT substitution can reduce electric leakage and thus enhance polarization.

Figure 6 shows the magnetic hysteresis loops (magnetization versus magnetic field) of BFO and BFO–5%BT at

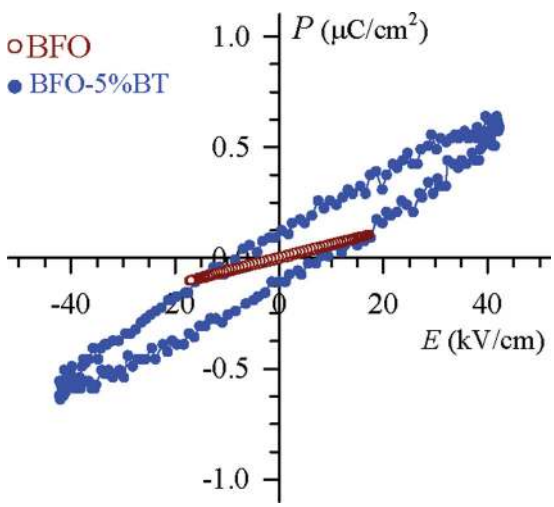

FIG. 5. (Color online) Hysteresis loops of electric polarization vs E field of BFO and BFO–5%BT at room temperature.

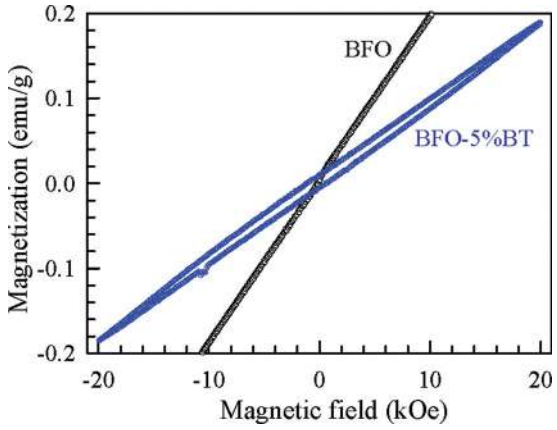

FIG. 6. (Color online) Hysteresis loops of magnetization vs magnetic field of BFO and BFO–5%BT at room temperature.

room temperature. The magnetization curve of BFO is linear with the field, which is typical for an antiferromagnetic arrangement of the Fe^{3+} magnetic moments. BFO–5%BT exhibits a rather weak ferromagnetic nature, which is similar to the magnetization curve observed in the BFO–10%BT ceramic.[29] These results suggest that BT substitution can enhance the FM feature.

IV. CONCLUSIONS

A local minimum in rhombohedral distortion angle α_R (associated with an inflection in the lattice constant a_R) was revealed near 400 and 350 °C in BFO and BFO–5%BT, respectively. The local minimum in α_R indicates that the position of Bi^{3+} reaches the largest distortion near T_N. This suggests a magnetoelectric coupling near T_N, which is responsible for the broad frequency dispersion in dielectric maxima. This work suggests that the Néel temperatures of BFO and BFO–5%BT are near 400 and 350 °C, respectively. A rhombohedral–orthorhombic–cubic transition sequence takes place near 820 and 850 °C in BFO upon heating. BFO–5%BT exhibits a rhombohedral–cubic transition near 830 °C. The dielectric loss of BFO–5%BT remains less than 0.04 below 150 °C, which is close to the $\tan\delta \cong 0.02$ of the soft PZT-5 ceramics.[34] The attainable polarization at room temperature was improved from ~0.01 $\mu C/cm^2$ in BFO to ~0.1 $\mu C/cm^2$ in BFO–5%BT. The 5%BT substitution can enhance dielectric and ferromagnetic responses.

ACKNOWLEDGMENTS

The authors would like to thank Dr. C.-S. Ku and Dr. H.-Y. Lee for their assistance on the synchrotron experiment. This work was supported by National Science Council of Taiwan Grant No. 97-2112-M-030-003-MY3.

[1]R. Ramesh and N. A. Spaldin, Nat. Mater. **6**, 21 (2007).
[2]N. Mathur, Nature **454**, 591 (2008).
[3]T. Choi, S. Lee, Y. J. Choi, V. Kiryukhin, and S.-W. Cheong, Science **324**, 63 (2009).
[4]*Handbook of Advanced Dielectric, Piezoelectric and Ferroelectric Materials*, edited by Z.-G. Ye (Woodhead, Cambridge, 2008).
[5]J. R. Teague, R. Gerson, and W. J. James, Solid State Commun. **8**, 1073 (1970).
[6]G. A. Smolenskii and I. Chupis, Sov. Phys. Usp. **25**, 475 (1982).
[7]R. Mazumder, S. Ghosh, P. Mondal, D. Bhattacharya, S. Dasgupta, N. Das, A. Sen, A. K. Tyagi, M. Sivakumar, T. Takami, and H. Ikuta, J. Appl. Phys. **100**, 033908 (2006).
[8]P. Fischer, M. Polomska, I. Sosnowska, and M. Szymański, J. Phys. C **13**, 1931 (1980).
[9]M. M. Kumar and V. R. Palkar, Appl. Phys. Lett. **76**, 2764 (2000).
[10]J.-C. Chen and J.-M. Wu, Appl. Phys. Lett. **91**, 182903 (2007).
[11]B. Ramachandran and M. S. Ramachandra Rao, Appl. Phys. Lett. **95**, 142505 (2009).
[12]J. M. Moreau, C. Michel, R. Gerson, and W. J. James, J. Phys. Chem. Solids **32**, 1315 (1971).
[13]R. T. Smith, G. D. Achenbach, R. Gerson, and W. J. James, J. Appl. Phys. **39**, 70 (1968).
[14]F. Kubel and H. Schmid, Acta Crystallogr., Sect. B: Structure Science **46**, 698 (1990).
[15]J. Li, J. Wang, M. Wuttig, R. Ramesh, N. Wang, B. Ruette, A. P. Pyatakov, A. K. Zvezdin, and D. Viehland, Appl. Phys. Lett. **84**, 5261 (2004).
[16]R. Palai, R. S. Katiyar, H. Schmid, P. Tissot, S. J. Clark, J. Robertson, S. A. T. Redfern, G. Catalan, and J. F. Scott, Phys. Rev. B **77**, 014110 (2008).
[17]G. Catalan and J. F. Scott, Adv. Mater. **21**, 2463 (2009).
[18]D. C. Arnold, K. S. Knight, G. Catalan, S. A. T. Redfern, J. F. Scott, P. Lightfoot, and F. D. Morrison, Adv. Funct. Mater. **20**, 2116 (2010).
[19]J. B. Neaton, C. Ederer, U. V. Waghmare, N. A. Spaldin, and K. M. Rabe, Phys. Rev. B **71**, 014113 (2005).
[20]P. Ravindran, R. Vidya, A. Kjekshus, H. Fjellvåg, and O. Eriksson, Phys. Rev. B **74**, 224412 (2006).
[21]D. Lebeugle, D. Colson, A. Forget, M. Viret, P. Bonville, J. F. Marucco, and S. Fusil, Phys. Rev. B **76**, 024116 (2007).
[22]V. V. Shvartsman, W. Kleemann, R. Haumont, and J. Kreisel, Appl. Phys. Lett. **90**, 172115 (2007).
[23]Y. P. Wang, L. Zhou, M. F. Zhang, X. Y. Chen, J. M. Liu, and Z. G. Liu, Appl. Phys. Lett. **84**, 1731 (2004).
[24]S. T. Zhang, M. H. Lu, D. Wu, Y. F. Chen, and N. B. Ming, Appl. Phys. Lett. **87**, 262907 (2005).
[25]G. L. Yuan and S. W. Or, Appl. Phys. Lett. **88**, 062905 (2006).
[26]W.-S. Kim, Y.-K. Jun, K. H. Kim, and S.-H. Hong, J. Magn. Magn. Mater. **321**, 3262 (2009).
[27]Z. X. Cheng, A. H. Li, X. L. Wang, S. X. Dou, K. Ozawa, H. Kimura, S. J. Zhang, and T. R. Shrout, J. Appl. Phys. **103**, 07E507 (2008).
[28]K. Sigh, R. K. Kotnala, and M. Singh, Appl. Phys. Lett. **93**, 212902 (2008).
[29]A. Singh, V. Pandey, R. K. Kotnala, and D. Pandey, Phys. Rev. Lett. **101**, 247602 (2008).
[30]M. M. Kumar, S. Srinath, G. S. Kumar, and S. V. Suryanarayana, J. Magn. Magn. Mater. **188**, 203 (1998).
[31]I. H. Ismailzade, I. M. Ismailov, A. I. Alekberov, and F. M. Salaev, Phys. Status Solidi A **68**, K81 (1980).
[32]B. D. Cullity, *Elements of X-Ray Diffraction* (Addison-Wesley, Reading, MA, 1978.
[33]Z. M. Tian, S. L. Yuan, X. L. Wang, X. F. Zheng, S. Y. Yin, C. H. Wang, and L. Liu, J. Appl. Phys. **106**, 103912 (2009).
[34]C. A. Randall, N. Kim, J.-P. Kucera, W. Cao, and T. R. Shrout, J. Am. Ceram. Soc. **81**, 677 (1998).
[35]A. Palewicz, R. Przenioslo, I. Sosnowska, and A. W. Hewat, Acta Cryst. B **63**, 537 (2007).